Anomalous Subdiffusion in Fluorescence Photobleaching Recovery: A Monte Carlo Study

Michael J. Saxton

Institute of Theoretical Dynamics, University of California, Davis, California 95616 USA

ABSTRACT Anomalous subdiffusion is hindered diffusion in which the mean-square displacement of a diffusing particle is proportional to some power of time less than one. Anomalous subdiffusion has been observed for a variety of lipids and proteins in the plasma membranes of a variety of cells. Fluorescence photobleaching recovery experiments with anomalous subdiffusion are simulated to see how to analyze the data. It is useful to fit the recovery curve with both the usual recovery equation and the anomalous one, and to judge the goodness of fit on log-log plots. The simulations show that the simplest approximate treatment of anomalous subdiffusion usually gives good results. Three models of anomalous subdiffusion are considered: obstruction, fractional Brownian motion, and the continuous-time random walk. The models differ significantly in their behavior at short times and in their noise level. For obstructed diffusion the approach to the percolation threshold is marked by a large increase in noise, a broadening of the distribution of diffusion coefficients and anomalous subdiffusion exponents, and the expected abrupt decrease in the mobile fraction. The extreme fluctuations in the recovery curves at and near the percolation threshold result from extreme fluctuations in the geometry of the percolation cluster.

INTRODUCTION

In normal diffusion, the mean-square displacement $\langle r^2 \rangle$ is proportional to time t. In anomalous subdiffusion, diffusion is hindered by obstruction or trapping in such a way that $\langle r^2 \rangle$ is proportional to some power of time less than one. That power α is the anomalous diffusion exponent.

Anomalous subdiffusion has been observed in membranes of several cell lines by various techniques. Single-particle tracking (SPT) measurements on the low-density lipoprotein receptor in human skin fibroblasts found that around half the particles showed anomalous subdiffusion, with values of α between 0.2 and 0.9 (Ghosh, 1991; Ghosh and Webb, 1994). Slattery (1995) reported anomalous subdiffusion of the high-affinity IgE receptor FcϵRI in rat basophilic leukemia cells measured by SPT, and Feder et al. (1996) measured anomalous subdiffusion in the same system by fluorescence photobleaching recovery (FPR). Sheets et al. (1997) used SPT to classify the motion of gold-labeled Thy-1 in fibroblasts. Trajectories in the fast class showed normal diffusion, but those in the slow and confined classes—61% of the trajectories examined—showed highly anomalous diffusion, with $\alpha = 0.42$ and 0.58, respectively. Simson et al. (1998) made similar SPT measurements on neural cell adhesion molecules in 3T3 and muscle cells. For NCAM-180 in 3T3 cells, 35% of the trajectories were classified as slow, with average $\alpha = 0.51$ and 21% corralled, with $\alpha = 0.29$. Schwille et al. (1999a,b) used fluorescence autocorrelation spectroscopy to measure anomalous subdiffusion of the IgE receptor and fluorescent lipid analogs in rat basophilic leukemia cells. They found $\alpha = 0.7–0.8$, though the experimental curve could be fit equally well assuming normal diffusion of two components. Smith et al. (1999) showed by SPT that in HeLa cells the class I major histocompatibility complex diffused anomalously with $\alpha = 0.49$.

If anomalous subdiffusion occurs it will have a major effect on mobility, and therefore on the kinetics of diffusion-mediated reactions. Fig. 1, suggested by a figure in Cherry et al. (1998), shows the effect of anomalous subdiffusion on the spread of diffusing particles from a point source.

The general effects of membrane heterogeneities on lateral diffusion are reviewed elsewhere (Saxton, 1999; Saxton and Jacobson, 1997). Many factors may be involved, and involved simultaneously: obstruction, binding, hydrodynamic interactions, interactions of extracellular domains, and interactions of intracellular domains with one another and with the membrane skeleton. For other recent reviews of membrane dynamics, see Edidin (1996, 1997), Jacobson and Dietrich (1999), and Kusumi and Sako (1996). Anomalous diffusion is reviewed by Bouchaud and Georges (1988, 1990), Bunde and Havlin (1991), Haus and Kehr (1987), Havlin and Ben-Avraham (1987), Havlin and Bunde (1991), and Shlesinger (1988).

Here we simulate FPR experiments with anomalous subdiffusion to answer three questions. Can anomalous subdiffusion be detected by FPR? How should the data analysis be done? How well can the diffusion coefficient and the anomalous diffusion exponent be measured? This work is based on the approximate treatment of anomalous subdiffusion by Feder et al. (1996), who viewed anomalous subdiffusion as resulting from random and continuously changing potential energy traps, with a wide range of binding energies yielding a range of escape times so wide that there is no average

Received for publication 26 April 2001 and in final form 16 July 2001.

Address reprint requests to Dr. Michael J. Saxton, Institute of Theoretical Dynamics, University of California at Davis, 1 Shields Ave., Davis, CA 95616-8618. Tel.: 530-752-6163; Fax: 530-752-7297; E-mail: mjsaxton@ucdavis.edu.

0006-3495/01/10/2226/15 $2.00

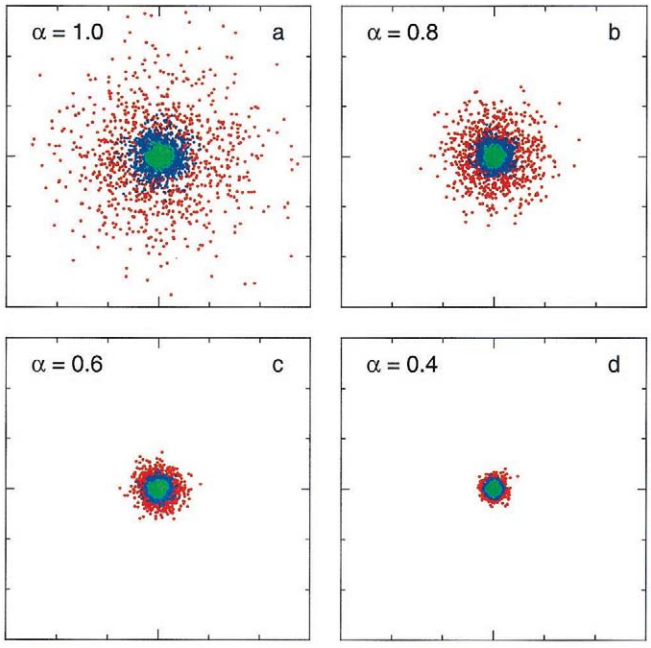

FIGURE 1 Effect of anomalous subdiffusion as α decreases from 1.0 (normal diffusion) to 0.4. One thousand tracers are placed at the origin and diffuse by a fractional Brownian motion algorithm (Lundahl et al., 1986). The position of each tracer is shown after 10 (*green*), 100 (*blue*), and 1000 (*red*) time steps. Note that there is relatively little effect at 10 time steps.

escape time. The traps could involve membrane proteins, lipids, cytoskeletal proteins, and the extracellular matrix.

We simulate FPR for diffusion in the presence of random point obstacles, for which diffusion is anomalous at the percolation threshold, and for two other models of anomalous subdiffusion, fractional Brownian motion (fBm) and the continuous-time random walk (CTRW). The results for obstructed diffusion are directly applicable to experiments on lateral diffusion in lipid mixtures in the region of lateral phase separation (reviews: Vaz, 1992; Almeida and Vaz, 1995). Percolation gives values of α between 0.697 and 1, so the other models are more appropriate for the extreme cases observed.

Simulations of FPR have been done by Coelho et al. (1997), Feder et al. (1996), Gordon et al. (1995), Nagle (1992), and Schram et al. (1994, 1996). We show that if one fits an anomalous recovery curve with the usual equation, the results are highly sensitive to the total measurement time, in agreement with the results of Nagle (1992). The results are much more consistent if the same data are fit with an equation that accounts for anomalous subdiffusion.

As in single-particle tracking (Saxton, 1997), scatter should be viewed as both signal and noise. The percolation threshold is marked by large scatter in the shape of the FPR recovery curves and in the resulting diffusion coefficients and anomalous subdiffusion exponents. The scatter results from variation in the geometric connectivity of the bleach region. In FPR measurements on cells and artificial bilayers, additional scatter may result from instrumental and biological factors. For reviews of instrumental factors see, for example, Gordon et al. (1995), Munnelly et al. (1998), Petersen et al. (1986), Thomas and Webb (1990), and Wolf (1989). Experimental results on scatter are summarized elsewhere (Saxton, 1997).

METHODS

We used Monte Carlo calculations to generate simulated recovery curves using an anomalous subdiffusion or normal random-walk algorithm. Both lattice and continuum simulations of FPR were used. The Tausworthe random number generator was used (Kirkpatrick and Stoll, 1981). Typically, 1000 tracers were used to generate each simulated recovery curve, and 500 recovery curves were generated. The system size was taken to be 512×512, and the bleach spot was a circle of radius 32 (containing 3697 points in the lattice simulations). A bleach spot of radius 48 or 64 gave distorted results in a 512×512 system. Periodic boundary conditions were imposed, but tracers contributed to the fluorescence signal only if they were in the bleach spot of the original 512×512 system, not if they were in a periodic image of the bleach spot. So, the obstructed system was, in effect, an infinite system with the obstacles periodically repeated.

A direct simulation of the FPR experiment would start unbleached tracers outside the bleach spot and measure whether they are in the bleach spot at various times. This is extremely inefficient, and one can considerably reduce the noise in the simulated recovery curve by starting bleached tracers inside the bleach spot and measuring their diffusion out of the bleach spot (Soumpasis, 1983; Coelho et al., 1997). This approach is valid for obstructed diffusion at low obstacle concentrations because the sum of the concentrations of bleached and unbleached tracers is constant. To verify that this works even in the case of anomalous subdiffusion, for which the diffusion coefficient is distance-dependent, two sets of runs were compared. In the standard runs, the tracers started inside the bleach spot in an infinite system. In the test runs, the tracers started outside the bleach spot in a finite system with conventional periodic boundary conditions. When tracers were started outside, 10,000 tracers were used to generate each simulated recovery curve, instead of 1000. The outside curves were still noisier than the standard curves; the computer time requirements for higher numbers of tracers would have been prohibitive. Tests were done for fBm, the CTRW, and obstructed diffusion at the percolation threshold. The difference in recovery curves between the two calculations was detectable, but not significant. The differences in the distributions of α and D were small compared with the width of the distributions, except that for the CTRW it was necessary to use 100,000 tracers in the outside runs.

The analytical expression for the recovery curve F(calc) was fit to the simulated curve F(sim). Anomalous subdiffusion requires a two-parameter fit using the equation $D(t) = \Gamma t^{\alpha-1}$ (Feder et al., 1996). Normal diffusion requires a two-parameter fit with the parameters D and the mobile fraction R_{mob}, though in almost all of the simulations here the actual mobile fraction is necessarily one. To eliminate possible errors from approximate data-fitting, the simulated recovery curves were fit to the full analytical expression for the recovery curve using the Levenberg-Marquardt nonlinear least-squares algorithm (Press et al., 1992). To prevent overflow it was useful to modify the subroutine of Press et al. (1992) for the modified Bessel function $I_\nu(z)$ to calculate $e^{-z}I_\nu(z)$ instead. In the least-squares fitting it was useful to constrain Γ to be positive (Gordon et al., 1995) by setting up the fitting equation in terms of $\sqrt{\Gamma}$. The fitting algorithm requires initial guesses for Γ and α, and in the simulations it is necessary to generate the initial guesses without manual intervention, even for noisy data. The best approach was to set up a grid of parameters spanning the entire reasonable range, calculate the error $\chi^2 = \Sigma[F(\mathrm{sim}) - F(\mathrm{calc})]^2$ for all values in that grid, and use as the initial guess Γ and α at the minimum χ^2. A second iteration of the grid search was useful. The coarse grid used $\alpha = 0.02$ to 2.0 by factors of $10^{1/5}$, and $\Gamma = 0.002$ to 100 in a 1/2/5

TABLE 1 Time sampling in simulations

Time range	Δt	Number of points	Weight
1–1K	1	1024	1
1K–4K	4	768	1024/768
4K–16K	16	768	1024/768
16K–64K	64	768	1024/768
64K–128K	256	256	16

progression. This search method is utterly inelegant but highly robust, and for analysis of thousands of noisy curves, robustness is essential. We will see in Results the range of curve shapes that must be accommodated. (An apparently reasonable alternative is to do least-squares fits of the initial and final segments of the recovery curves to polynomials in t found from the series expansion of the exact solution. The grid search was preferable.)

Each simulated recovery curve included 2000–8000 time points, closely spaced at short times and widely spaced at long times. Even with this time sampling, appropriate weighting of the time segments is necessary. A long run is required to approach full recovery, particularly in anomalous subdiffusion. However, if a long run is sampled at equal time intervals and fit with the time points equally weighted, the slow final approach to full recovery is given much more emphasis than the initial part of curve where most of the change takes place. The time sampling and weighting are shown in Table 1 for a run of 128K time points ($1K = 1024$) sampled at time intervals Δt, for a total of 3584 time points. A similar pattern was used for larger numbers of time points. Gordon et al. (1995) used a time-dependent smoothing algorithm with a similar effect. The weighting was chosen so that the first and the last halves of the time points (1 to 64K and 64K to 128K) are weighted equally, and the four segments in the first half are weighted equally. (This method leads to artifactual changes in the noise among segments, as will be seen in some of the figures.) The obvious alternative, weighting time points inversely according to the noise in the segment, would not work. Such an approach would just place very heavy weight on the points for large t. In analyzing experimental data one might record the recovery curves at equal intervals of log t instead of t (Donaldson, 1989) and weight them appropriately.

Obstructed diffusion on a lattice was modeled as described before (Saxton, 1996). Briefly, mobile point obstacles were placed on a triangular lattice at random at a prescribed concentration. The infinite percolating cluster was identified by the algorithm of Hoshen and Kopelman (1976). A tracer was placed at a random unblocked lattice point on the infinite cluster inside or outside a circular bleach spot, as required, and carried out a random walk on unobstructed lattice sites. The tracer position was recorded as a function of time. The approximations involved in a lattice model of lateral diffusion are discussed by Scalettar and Abney (1991) and by Almeida and Vaz (1995).

The CTRW was modeled as described elsewhere (Saxton, 1996) for lattice diffusion, though some continuum calculations were also done as a control. In the continuum calculations, the direction of the step was chosen randomly from a uniform distribution and the length was chosen randomly from the distribution $\exp(-r^2/4Dt)\,2\pi r dr$. The time scale for the CTRW is different from the other two models, as will be seen in some of the figures.

Modeling fractional Brownian motion requires care. Many methods have been proposed in the literature, some suitable for quantitative tests of the accuracy of methods of analyzing fractal dimensions, and others mostly useful for generating fractal landscapes (for reviews see Caccia et al. (1997); Jennane et al. (1996)). One high-quality method is to generate Gaussian random variates and then directly put in the required correlations (Lundahl et al., 1986). The original method requires a $N \times N$ correlation matrix to generate a time series of N points, but a more recent version (Falconer and Véhel, 2000) is more practical. The fractional Gaussian process algorithm recommended by Caccia et al. (1997) requires too many Gaussian random variates to be practical here. Instead, we used another high-quality method, the Weierstrass-Mandelbrot (WM) function (Berry and Lewis, 1980; Feder, 1988; Molz et al., 1997; Voss, 1988)

$$W_x(t) = \sum_{n=-\infty}^{+\infty} \frac{1}{\gamma^{nH}} (\cos \phi_x(n) - \cos[\gamma^n t^* + \phi_x(n)]), \quad (1)$$

where t is time, t_{max} is the total time, $t^* = 2\pi t/t_{max}$, $\gamma > 1$ is a constant here chosen to be $\sqrt{\pi}$ (Jaggard, 1990), and $\phi_x(n)$ are random phases uniformly distributed between 0 and 2π. In a Fourier series the terms form an arithmetic series in the frequency; here the terms form a geometric series. As n increases, the frequencies increase and the amplitudes decrease. The geometric variation in frequency produces structure on all time scales, as is required for $W_x(t)$ to be fractal (Molz and Boman, 1995). The WM function gives the x-position of the tracer at time t. (To generate fractional Brownian noise one would take differences of $W_x(t)$, and to generate fractional Brownian motion from the noise one would sum the noise, regenerating $W_x(t)$.) The y-position is obtained similarly, but with independent random phases. A normalization factor was chosen to make the step size at unit time $\langle r^2 \rangle = 1$. In the simulations, the sum in Eq. 1 was taken from -8 to $+48$. These values were chosen by examining the ratio $\langle r^2 \rangle / t$ for normal Brownian motion, $H = 1/2$. If the lower limit is -4, the ratio droops around 2 million time steps; if -8, the ratio oscillates around a constant value. Adding more terms on either end of the series has little effect. The reason for the oscillation is as follows. If one evaluates W_x^2 and averages over the random phases, one obtains

$$W_x^2(t) = \sum_{n=-\infty}^{+\infty} \frac{1}{\gamma^{2nH}} [1 - \cos(\gamma^n t^*)], \quad (2)$$

which is the WM function of Eq. 1 with the random phases zero and an exponent $2H$ instead of H.

In some of the figures, Catmull-Rom splines (Foley et al., 1990) were used to draw smooth curves through data points. This is a convenient way to produce curves like the smooth curves one would sketch by hand.

RESULTS

Theoretical recovery curves: equations

In anomalous subdiffusion the mean-square displacement is

$$\langle r^2 \rangle \sim t^\alpha \quad (3)$$

in the limit of large t with the anomalous diffusion exponent $\alpha \leq 1$. So the diffusion coefficient D is time-dependent:

$$D(t) \propto \langle r^2 \rangle / t \sim t^{\alpha - 1}. \quad (4)$$

These equations hold only in the limit of large t, but we shall use the same asymptotic approximation that the Webb group used (Feder et al., 1996), and assume that Eq. 4 holds for all $t \geq 1$, so that

$$D(t) = \Gamma t^{\alpha - 1}, \quad (5)$$

with Γ constant. If $\alpha = 1$, $\langle r^2 \rangle \sim t$, $D = \Gamma$ is constant, and diffusion is normal. As we shall see, Eq. 5 is an approximation, but it captures much of the behavior of anomalous subdiffusion.

When Eq. 5 is used for $D(t)$, one can use the standard expressions for the recovery curves with $D(t)$ substituted for D. To show this we outline how the equation for the normal

recovery curve can, in principle, be derived. (In practice, the integrals are intractable and transform methods are used.) The propagator or Green's function for diffusion $G(r, r', t, 0)$ gives the concentration of diffusing species at a position r at time t due to a point source at a position r' at time 0. For normal diffusion in two dimensions, $G(r, r', t, 0) = (1/4\pi Dt)\exp[-(r - r')^2/4Dt]$. We start with an initial distribution of label $C(r', 0)$ and integrate over r' to give the distribution of label at time t, $C(r, t) = \int G(r, r', t, 0)C(r', 0)d\mathbf{r}'$. Then we find the fluorescence by multiplying $C(r, t)$ by the beam intensity $I(r)$ and integrating over r, giving $F(t) = \int C(r, t)I(r)d\mathbf{r}$. The derivation for the anomalous recovery curve would be done similarly. Now D and t occur only as the product Dt, and this factor has no effect on the integrations over $\mathbf{r}'$ and $\mathbf{r}$. So in the approximation of Eq. 5 one can just use the standard derivation of $F(t)$ and replace Dt with Γt^α at the end.

The bleach beam is assumed to be circular and of uniform intensity, not Gaussian, and the equation of Soumpasis (1983) is used for the recovery curve:

$$F(z) = e^{-z}[I_0(z) + I_1(z)], \tag{6}$$

where $z = 2\tau_D/t$, $\tau_D = w^2/4D$ is the characteristic time for recovery, w is the beam radius, D is the diffusion coefficient, and $I_\nu(z)$ is a modified Bessel function. Other forms of $F(z)$ and their relation to Eq. 6 are discussed in the Appendix. The same assumptions were made in the analysis of experiments on lipid mixtures (Almeida and Vaz, 1995; Vaz, 1992).

Theoretical recovery curves: qualitative behavior

It is useful to look at the form of the recovery curves in the limits of long and short times. At short times (Soumpasis, 1983),

$$F(z) = \sqrt{\frac{4Dt}{\pi w^2}}\left[1 - \frac{1}{16}\frac{4Dt}{w^2} + \cdots\right] \tag{7}$$

so that the initial time dependence is

$$F(t) = \sqrt{\frac{4\Gamma t^\alpha}{\pi w^2}} + \cdots. \tag{8}$$

For normal diffusion, this gives $F(t) \propto t^{1/2}$. At long times (Soumpasis, 1983),

$$F(t) = 1 - \frac{w^2}{4Dt} + \left(\frac{w^2}{4Dt}\right)^2 - \cdots \tag{9}$$

so that in the anomalous case

$$F(t) = 1 - \frac{w^2}{4\Gamma t^\alpha} + \cdots. \tag{10}$$

The effect of α in Eq. 10 can be significant. For example, at the percolation threshold, where $\alpha = 0.697$ (Havlin and Bunde, 1991), the time needed for $1/t^\alpha$ to reach 0.01 is $t \simeq 740$ instead of 100.

Fig. 2 shows families of recovery curves for normal diffusion and anomalous subdiffusion from Eqs. 5 and 6 as linear and log-log plots. The linear plots of anomalous subdiffusion show the slow approach to complete recovery observed experimentally (Almeida and Vaz, 1995; Vaz, 1992). The log-log plots are much more revealing. In normal diffusion, the initial slope is always 1/2, the final value is here $F(\infty) = 1$, and varying D simply changes the intersection of the two limiting lines. In the anomalous case, the initial slope is $\alpha/2$ and the rate of approach to $F(\infty) = 1$ is set by α. As we shall see, freedom to vary the initial slope is essential in fitting Monte Carlo anomalous recovery curves. Equations 5 and 6 require that the initial and final slopes of the log-log plots be proportional. Note that in a pure anomalous subdiffusion model the mobile fraction is necessarily 1, though the time to reach that limit may be long. Changing Γ at constant α shifts the anomalous curves just as shifting D does for the normal recovery curves.

Models of anomalous subdiffusion

We shall use several models of anomalous subdiffusion in the simulations, to cover the full range of α reported in cell membranes, to avoid model dependence, to test for artifacts, and to illustrate the differences in commonly used models of anomalous subdiffusion. It would be premature to focus entirely on one model because the cause of anomalous subdiffusion in biological membranes has not been established, and several factors are likely to be involved simultaneously, as in the obstruction-binding model (Saxton, 1996). We consider obstructed diffusion, fBm, and CTRW, but not binding.

Obstructed diffusion is one of the standard models of hindered diffusion, and is of interest because lipid mixtures can provide a direct physical realization. In an unobstructed system, diffusion is normal. As obstacles are added, diffusion becomes anomalous at short times and normal at long times. As the obstacle concentration C increases to the percolation threshold C_P, the crossover from anomalous to normal diffusion takes place at longer and longer times, and diffusion becomes more anomalous. At the threshold, the crossover time becomes infinite. A percolation cluster is self-similar—that is, it has no characteristic length scale—so diffusion on a percolation cluster has no characteristic time scale. Diffusion on a percolation cluster is therefore anomalous at all times, except for the first few time steps, where the nonzero lattice or obstacle spacing affects diffusion. A tracer diffusing on a percolation cluster encounters dead ends, bottlenecks, obstructed areas, and other hindrances to diffusion on all length scales; these hindrances lead to anomalous subdiffusion. Obstructed diffusion provides only a narrow range of α. When $C = 0$, $\alpha = 1$, and when $C = C_P$, $\alpha = 0.697$. For intermediate obstacle concentrations, α varies smoothly between these values

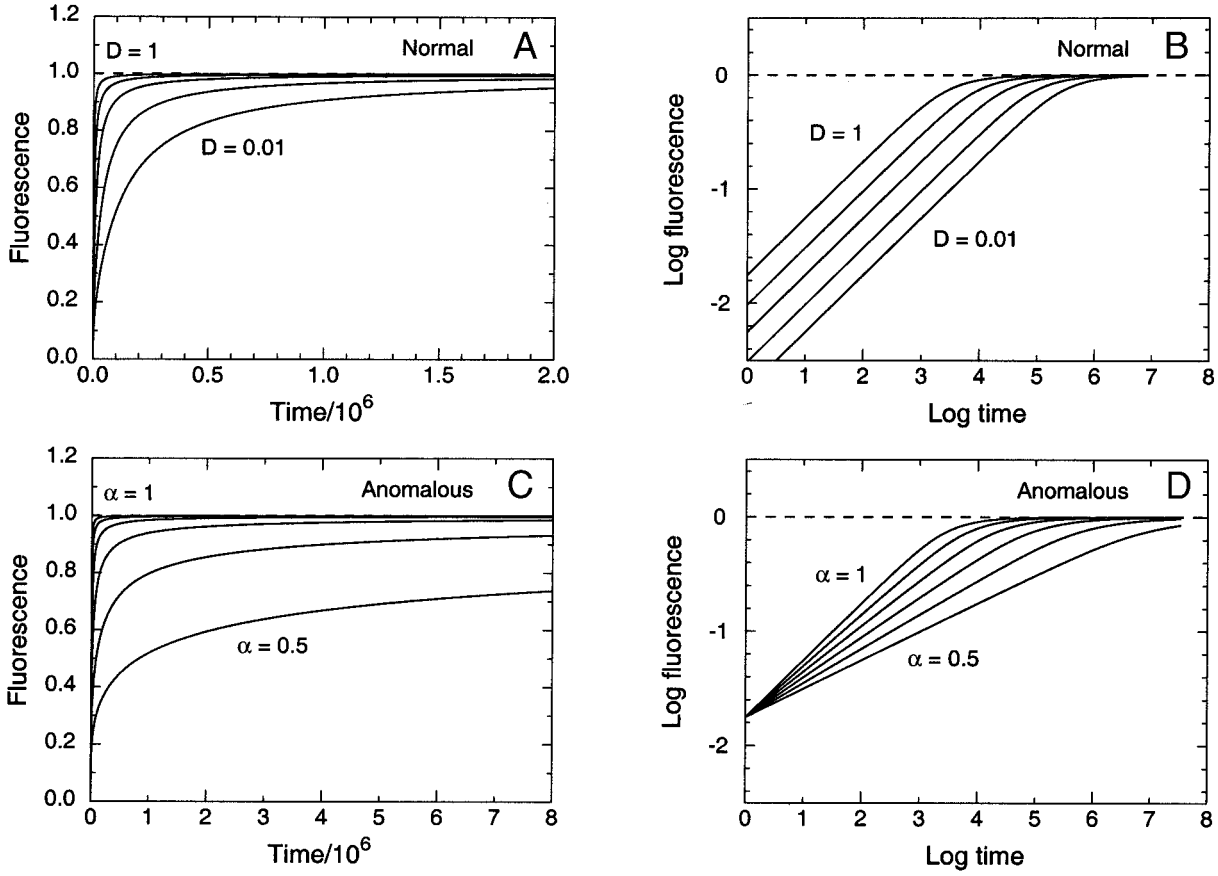

FIGURE 2 Theoretical recovery curves for normal diffusion and anomalous subdiffusion. Note the difference in time scales between (*a*) and (*c*). *Dashed horizontal lines*, full recovery. (*a*) Normal recovery curves for $D = 0.01$, 0.03, 0.1, 0.3, and 1; mobile fraction 1.0. (*b*) Log-log plot of the same normal recovery curves. (*c*) Anomalous recovery curves for $\alpha = 0.5$, 0.6, 0.7, 0.8, 0.9, 1.0, with $\Gamma = 1$. (*d*) Log-log plot of the same anomalous recovery curves.

(Saxton, 1994). (There the exponent is given as $d_w = 2/\alpha$, the usual notation in the physics literature.)

Near the percolation threshold, there is one infinite cluster of conducting sites ("ocean") and many finite clusters of conducting sites ("lakes"). If a lake is entirely within the bleach spot, no recovery occurs and the lake contributes to the immobile fraction. If a lake crosses the edge of the bleach spot, the lake contributes to fast recovery. To ensure the purest anomalous subdiffusion at the threshold, we restrict tracers to the ocean, thus requiring that there is no immobile fraction. A justification for this restriction is that smaller lakes are more common; the number n_s of lakes containing s points is $n_s \sim s^{-2.055}$ (Stauffer and Aharony, 1992). So there could be a significant contribution to recovery from tracers in lakes of size two or three lattice points straddling the bleach spot boundary. Including this recovery would be pressing a lattice model of diffusion beyond the reasonable. To eliminate lakes experimentally, one could do a long preliminary bleach to deplete the tracer in the lakes (Schwille et al., 1999a).

The CTRW is a standard model from physics (Scher et al., 1991). In a CTRW the diffusing particle carries out an ordinary random walk, but with a modified time scale. At each step in a normal random walk the time is incremented by $\Delta t = 1$, but in a CTRW, Δt is a random waiting time chosen from a singular distribution

$$\psi(t) = \beta/(1 + \Delta t)^{1+\beta} \tag{11}$$

(Scher et al., 1991) and

$$\langle r^2 \rangle \sim t^{\beta} \tag{12}$$

for large t (Blumen et al., 1984). The system has no memory; if a tracer escapes from the same point several times, the escape times are independent. The CTRW gives temporal disorder with no spatial dependence, but a random walk on a percolation cluster gives spatial disorder with no time dependence. Nagle (1992) used the CTRW to analyze the effect of long-time tails in the jump rate on one-dimensional FPR. He showed that the diffusion coefficient and the fractional recovery varied strongly with the measurement time.

Another model we use is fBm on a continuum. Normal diffusion on the continuum is driven by white noise, but fBm is driven by correlated noise. The correlation is specified by the Hurst exponent H, with $H = 1/2$ corresponding

to uncorrelated motion, that is, normal diffusion. The mean-square displacement is proportional to t^{2H} (Feder, 1988).

We do not consider anomalous subdiffusion due to binding because the simulations required are much different. One would use multiple tracers that exclude other tracers from their position. Tracers in deep traps would not contribute to fluorescence recovery, but would obstruct other tracers. Diffusion would be sensitive to the tracer concentration, because the tracer concentration would determine the deepest unfilled trap. Diffusion in such a system would also depend critically on whether the tracer is in thermal equilibrium with the traps (Saxton, 1996).

Noise in models

The obstructed diffusion model translates most directly into a biophysical model. Vaz, Thompson, Almeida, and their collaborators used FPR to measure lateral diffusion in binary and ternary lipid mixtures in the region of lateral phase separation. They presented their results as plots of the mobile fraction as a function of the area fraction of gel phase from the phase diagrams. They observed clear percolation thresholds and found major differences in thresholds for different lipid mixtures, attributed to differences in the geometry of the gel phases among the mixtures (reviews: Vaz, 1992; Almeida and Vaz, 1995).

Coelho et al. (1997) modeled these experiments as a random walk in the presence of overlapping, randomly oriented elliptical obstacles, and generated simulated recovery curves. The main object was to find domain sizes and axial ratios of ellipses that would reproduce the observed values of the fractional recovery as a function of the area fraction of fluid phase, and would be consistent with other estimates of domain size (Almeida et al., 1993).

In these experiments and simulations, the FPR recovery curves were fit using the equation of Soumpasis (1983) for normal diffusion, plus a linear ramp if required. Originally, the ramp was taken to represent recovery due to diffusion in defects in the gel phase (Vaz et al., 1989), but the ramp could also represent slow diffusion due to percolation (Coelho et al., 1997). Slow diffusion could result from, say, diffusion between "lakes" joined by a narrow "strait." As Eq. 10 indicates, a ramp is a natural consequence of an anomalous subdiffusion model. This model predicts that the ramp would be required only near the percolation threshold, in the region where α is significantly less than one.

Furthermore, the scatter in the mobile fraction was high near the percolation threshold (Almeida et al., 1992b). Noise near the threshold is a consequence of a percolation model. A percolation cluster at the threshold is shown in Fig. 3, along with three arbitrarily chosen bleach spots. Two sources of fluctuations are evident. First, the number of conducting sites in the bleach spot varies considerably, though in experiments this variation is removed by normalizing the recovery curve $F(t)$ by the prebleach fluorescence

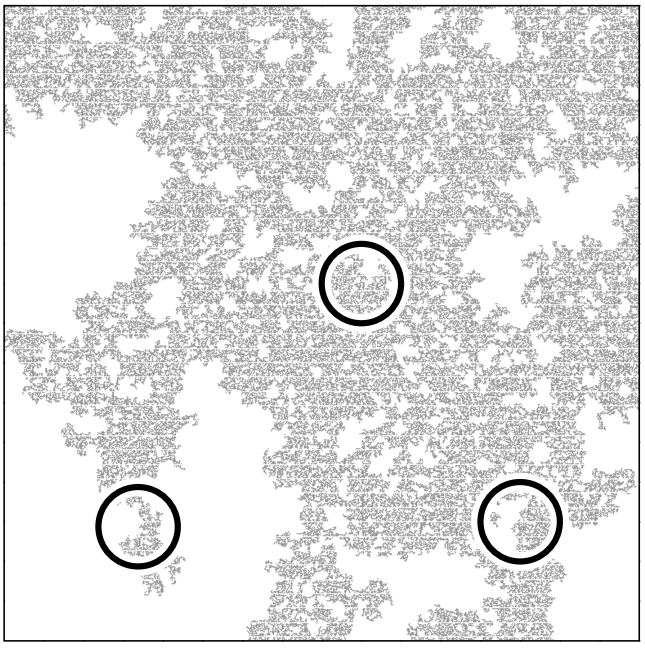

FIGURE 3 A percolation cluster with arbitrary bleach spots. The percolation cluster is on a triangular lattice at the threshold $C_P = 0.5$. This is at the scale used in the simulations, a 512 × 512 cluster with a bleach spot of radius 32.

$F(-)$. Second, there is great variation in the connectivity of the bleach spot to the rest of the cluster. This is significant, leading to the variation in recovery curves shown in Fig. 4.

There are, however, two important differences between the experiments and the simulations in Fig. 4. First, the simulations exclude diffusion on nonpercolating clusters and fast recovery in lakes at the edge of the bleach spot. The fast recovery affects the shape of the initial part of the

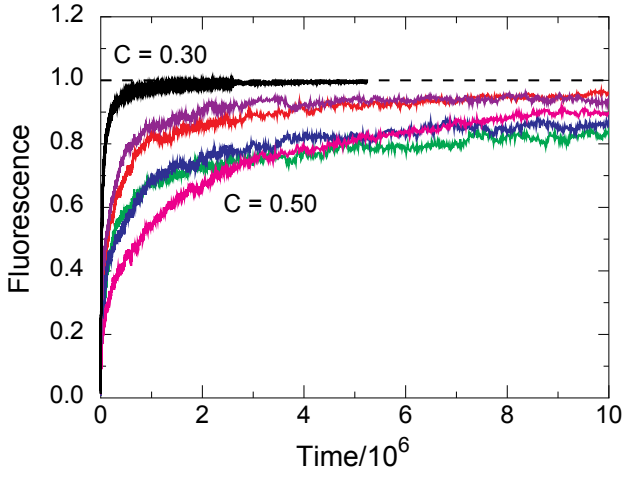

FIGURE 4 Scatter among five simulated FPR curves for obstructed diffusion with $C = 0.3$ (*black*) and five curves with $C = C_P = 0.5$ (*color*). The abrupt changes in noise level are artifacts of the time sampling used (see Methods).

recovery curve, and recovery in lakes introduces significant variation in the mobile fraction. If the lakes are excluded, all conducting sites are on the percolation cluster and $F(\infty) = 1$, but if they are included, $F(\infty)$ depends on the ratio of lake sites to ocean sites in the bleach spot, and the extent to which the lakes overlap the bleach spot. Second, the experiments were on multilayers containing hundreds of bilayers, but the simulations used single configurations of obstacles, corresponding to a single bilayer. Almeida et al. (1992b) suggested that the observed fluctuations may occur because each bilayer in the stack is either percolating or not percolating.

The sets of simulated FPR curves of Fig. 4 are anecdotal evidence about noise. We can characterize the noise more systematically by calculating the standard deviation of the recovery curve, as shown in Fig. 5. The recovery curves are highly reproducible well below the threshold ($C = 0.0$ and 0.3) but are extremely scattered at the threshold. The standard deviation at the threshold is even larger if lakes and nonpercolating clusters are included. Note that a plot of the standard deviation tends to sanitize the results. The results in Fig. 5 *a* for $C = 0.5$ would be consistent with a single reproducible recovery curve with a large amount of high-frequency noise, but Fig. 4 implies that the problem is instead low-frequency noise leading to major variations in the entire recovery curve, including ramps.

In contrast, there is much less scatter for fBm and the CTRW as shown in Fig. 5, *b* and *c*. The plots in Fig. 5 are strictly comparable: 500 recovery curves were simulated, 1000 tracers were used per recovery curve, and the recovery curves for $C = C_P = 0.5$, $2H = 0.697$, and $\beta = 0.697$ all have in the asymptotic limit a mean-square displacement $\langle r^2 \rangle \sim t^{0.697}$.

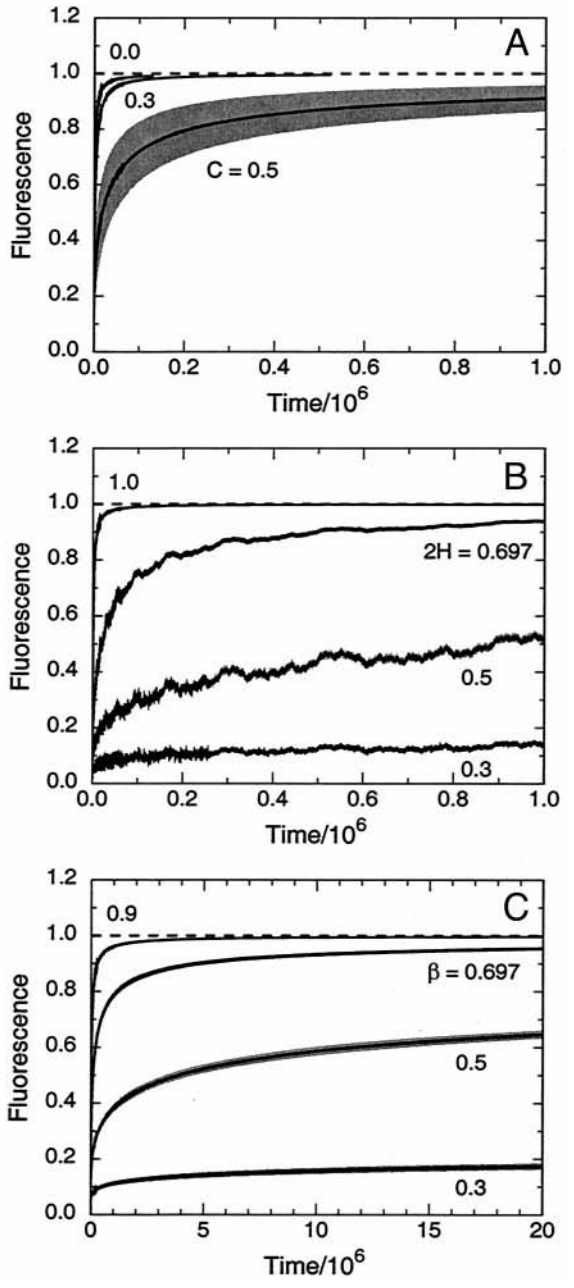

FIGURE 5 Standard deviation of FPR recovery curves for 500 recovery curves with 1000 tracers per recovery curve. *Lines*, mean recovery curve. *Gray area*, mean recovery curve ± one standard deviation. (*a*) Obstructed diffusion with $C = 0.0$, $C = 0.3$, and $C = C_P = 0.5$. (*b*) fBm with $2H = 0.300$, 0.500, 0.697, and 1.000. Note the oscillations of increasing period, most evident in the curve for $2H = 0.500$. (*c*) CTRW with $\beta = 0.300$, 0.500, 0.697, and 0.900.

Fitting individual recovery curves

To test the fit of normal and anomalous curves to the simulated recovery curves, it is helpful to use linear plots to emphasize the behavior at large t, and log-log plots to emphasize small t. Fig. 6 shows least-squares fits of both of the theoretical curves to simulated recovery curves. In Fig. 6, *a* and *b*, for obstructed diffusion at the percolation threshold, it is clear from the linear plot that the anomalous curve gives a better fit than the standard recovery curve. The log-log plot shows that the problem with the standard fit is that the initial slope is fixed at 1/2, so the curve is too low at small t and then overshoots the recovery curve. But the least-squares fit to the anomalous curve gives an initial slope of 0.35 and this leads to a much better fit. The anomalous curve does not always fit this well, but it is in general a significant improvement over the standard curve.

For fBm with $2H = 0.697$, the anomalous curve fits better than the standard curve, as is clear in both linear and log-log plots (Fig. 6, *c* and *d*). The freedom to vary the initial slope in the log-log plot is crucial to the good fit.

For the CTRW with $\beta = 0.697$, the linear plot Fig. 6 *e* shows that the anomalous curve unquestionably gives a better fit, but the log-log plot in Fig. 6 *f* shows a deviation in the fit at small times. As the average recovery curve in Fig. 6 *f* shows more clearly, there are three segments of approximately constant slope in the CTRW recovery curve, and the least-squares fit deviates at small t. This structure of the recovery curve does not appear to be artifactual; the same structure was obtained with contin-

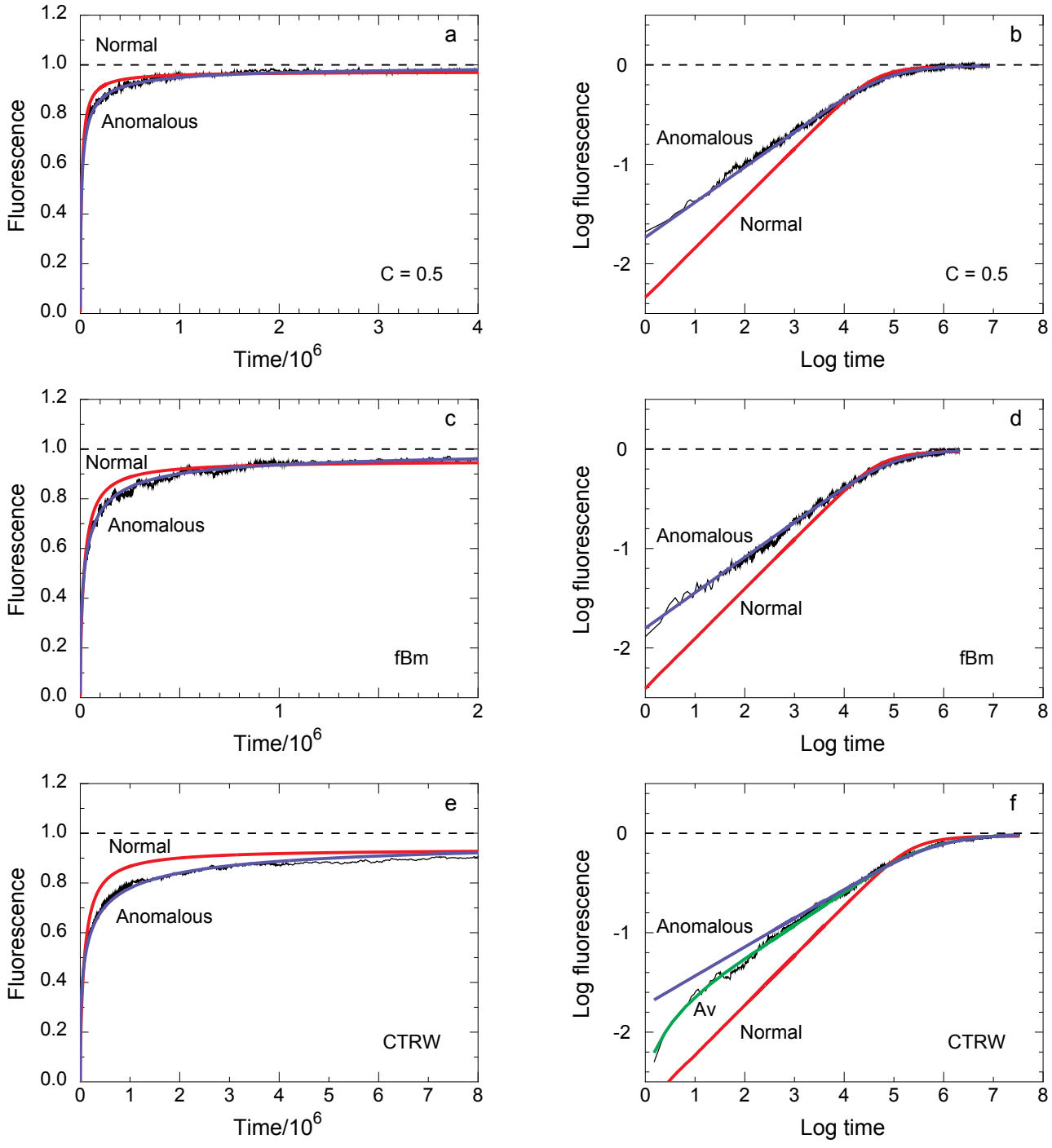

FIGURE 6 Simulated recovery curves (*black*) and least-squares fits to them using the normal (*red*) and anomalous (*blue*) equations. Recovery curves are for 1000 tracers. Note the different time scales in the linear plots. (*a*, *b*) Obstructed diffusion with $C = C_P = 0.5$. Linear and log-log plots. (*c*, *d*) fBm with $2H = 0.697$. Linear and log-log plots. (*e*, *f*) CTRW with $\beta = 0.697$. Linear and log-log plots. In *f* the average recovery curve over 500 grids (*green*) is also included to show that the structure at short times is real, not just noise in the particular curve shown.

uum diffusion and with the ran2 random number generator (Press et al., 1992).

Why are the simulated recovery curves different in the different models? Anomalous subdiffusion simply requires that at large times $\langle r^2 \rangle \sim t^\alpha$, but does not specify either the behavior at short times or the behavior of higher moments of r. One can examine the differences in the models by plotting $\langle r^2 \rangle / t^\alpha$, which approaches a constant at large t. For unobstructed diffusion $\alpha = 1$, and for obstructed diffusion at the percolation threshold $\alpha = 0.697$. We choose the

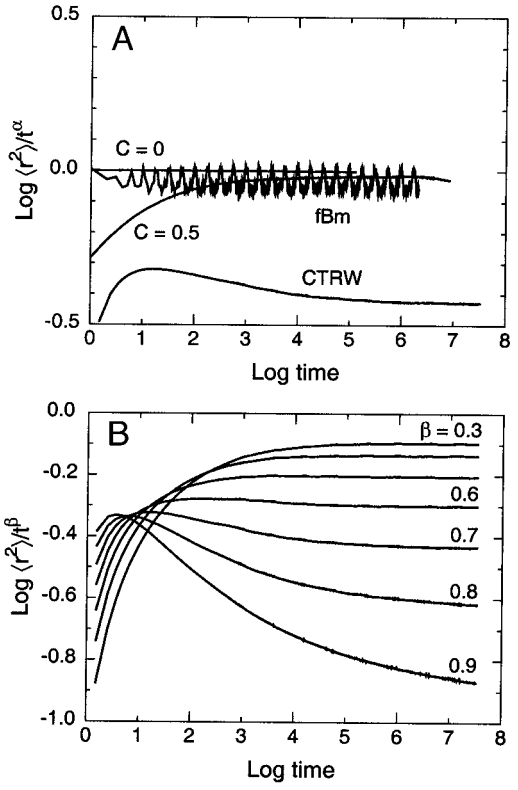

FIGURE 7 Scaled moments $\langle r^2\rangle/t^\alpha$. (*a*) Moments for unobstructed diffusion ($C = 0$, $\alpha = 1$), obstructed diffusion at the percolation threshold ($C = 0.5$, $\alpha = 0.697$), fBm with $2H = 0.697$, and the CTRW with $\beta = 0.697$. The unobstructed case is continuum diffusion with a random step size as described in Methods for the continuum CTRW. (*b*) Moments for the CTRW with $\beta = 0.3$, 0.4, 0.5, 0.6, 0.7, 0.8, and 0.9.

parameters $2H$ and β in the other models so that they have the same asymptotic behavior as in percolation.

Results are shown in Fig. 7 *a*. For unobstructed diffusion, $C = 0$, $\log\langle r^2\rangle/t = 0$ for all times. All three anomalous curves are horizontal at large times, as required by the asymptotic limit, but the behavior at short times is much different. (The most prominent oscillations in the fBm curve are of frequency γ, from the $n = -1$ term in Eq. 2.) In terms of this plot, Eq. 5 is an approximation in which it is assumed that $\langle r^2\rangle/t^\alpha$ is constant for all $t > 1$. It describes the asymptotic behavior correctly, but does not include the short-time behavior of the anomalous subdiffusion models. Plots for higher moments $\langle r^{2n}\rangle/t^{n\alpha}$, $n = 2$, 3, and 4, are of similar shape, but with vertical shifts in the absolute and relative positions.

Fig. 7 *b* shows similar curves for the CTRW as β is varied. For highly anomalous subdiffusion, say $\beta = 0.3$ as used by Nagle (1992), $\langle r^2\rangle/t^\beta$ reaches its asymptotic value quickly and the asymptotic approximation Eq. 5 works well. However, as diffusion becomes less anomalous, say $\beta = 0.8$, the approach is much slower. The entire recovery curve then falls in the initial region, and Eq. 5 does not work well. (If the simulations are repeated with a larger beam radius and system size, more of the recovery curve is in the asymptotic region. The fit and the values of α are better, though very large systems must be used.)

Anomalous subdiffusion exponents

How well can the anomalous subdiffusion exponent α be determined in an FPR measurement? Fig. 8 *a* gives the mean values of α for obstructed diffusion. As a reference value we show α_{RSQ}(init), determined from the initial slope of a plot of $\log\langle r^2\rangle$ versus $\log t$. As the obstacle concentration C increases from 0 to the percolation threshold C_P, the short-range α_{RSQ}(init) decreases smoothly from 1 at $C = 0$ to 0.697 at C_P (Saxton, 1994); but α_{FPR} from the recovery curves is a longer-range value measured over a length of the order of the beam width, and remains at 1 until the system is near C_P. As a result, in the histogram in Fig. 8 *b*, values of α_{FPR} are distributed around 1 for $C \leq 0.3$. A slight shift toward lower values begins at $C = 0.3$, and a significant change occurs around $C = 0.4$. The distribution broadens considerably as the obstacle concentration approaches the percolation threshold. For fBm the distributions of α are narrow and the means are very close to the true values. For the CTRW the distributions are similarly narrow, but the means are incorrect except for small β. The cause of the problem is the slow approach of $\langle r^2\rangle$ to its asymptotic value, shown in Fig. 7 *b*. Unfortunately, fits to the CTRW model give diffusion more anomalous than is correct.

Diffusion coefficients

In anomalous subdiffusion the diffusion coefficient is time-dependent, but it would be convenient to be able to refer to a single diffusion coefficient. One solution is to discuss all results in terms of D(1 s) (Feder et al., 1996), but this seems arbitrary. An alternative is to define a single value of D self-consistently in terms of the bleach radius w. We have from Feder et al. (1996)

$$\langle r^2\rangle = \Gamma t^\alpha \tag{13}$$

and

$$D(t) = \tfrac{1}{4}\Gamma t^{\alpha-1}. \tag{14}$$

Define τ as the time at which $\langle r^2\rangle = w^2$, evaluate the equations at time τ, and eliminate τ to give

$$D(w) = \frac{1}{4}\Gamma\left(\frac{w^2}{\Gamma}\right)^{(\alpha-1)/\alpha}. \tag{15}$$

or

$$D(\tau) = \tfrac{1}{4}\Gamma\tau^{\alpha-1}. \tag{16}$$

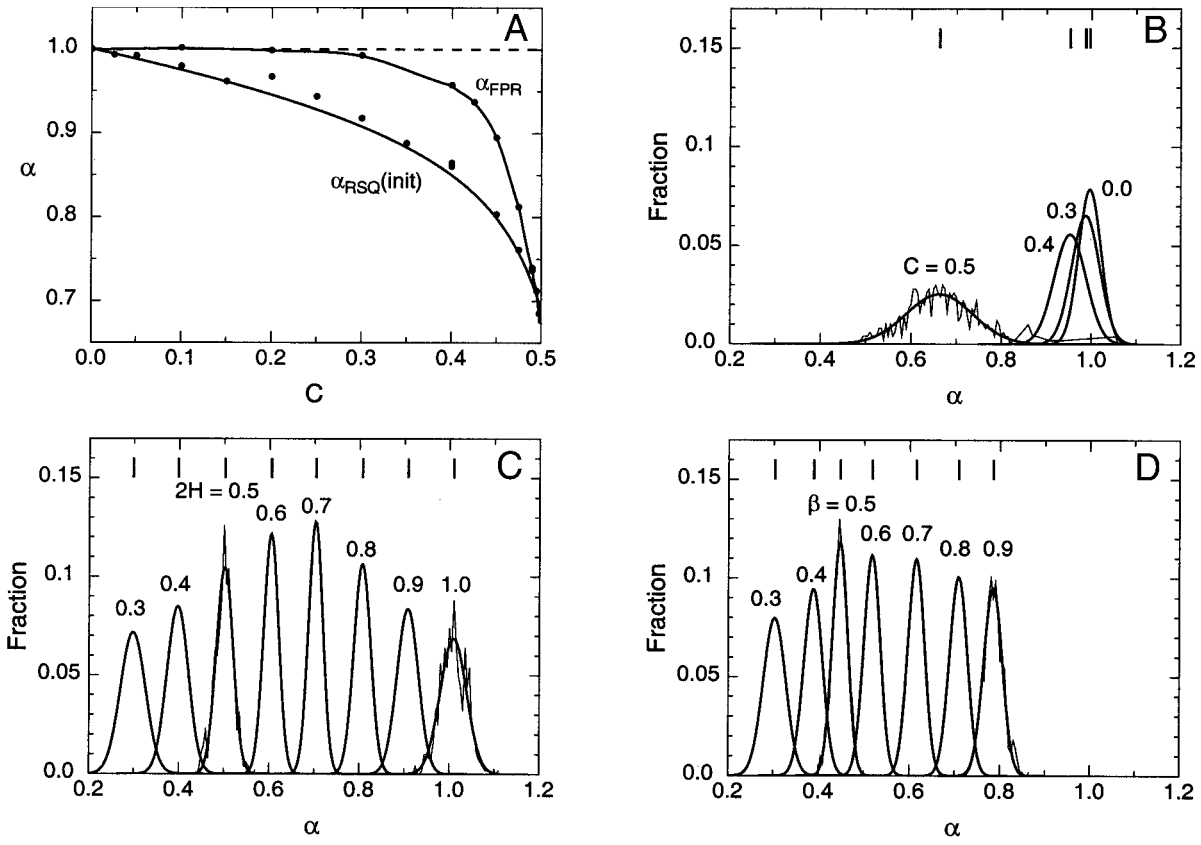

FIGURE 8 Distributions of anomalous subdiffusion exponents α for simulated recovery curves fit by Eqs. 5 and 6. The smooth curves are Gaussians fit to the observed histograms; for some distributions, the actual histogram is shown as a fine line. The short vertical lines are mean values. (*a*) Mean anomalous diffusion exponent α as a function of obstacle concentration C. Here α_{RSQ}(init) is the short-range value from fits to the initial slope of log $\langle r^2\rangle$ versus log t, and α_{FPR} is the long-range value from the FPR simulations. The line for α_{RSQ}(init) is a least-squares fit to $2/\alpha$ given elsewhere (Saxton, 1994), and the line for α_{FPR} is a Catmull-Rom spline. (*b*) Obstructed diffusion with $C = 0.0$, 0.3, 0.4, and $C = C_P = 0.5$. (*c*) fBm with $2H = 0.3$, 0.4, 0.5, 0.6, 0.7, 0.8, 0.9, and 1.0. (*d*) CTRW with $\beta = 0.3$, 0.4, 0.5, 0.6, 0.7, 0.8, and 0.9.

For normal diffusion, $\alpha = 1$ and $D(w) = \frac{1}{4}\Gamma$ is constant. In the Monte Carlo calculations, $D(w)$ is normalized to eliminate the factor of ¼.

We define two diffusion coefficients based on Eq. 15: $D_{RSQ}(w)$ is obtained from fitting Eq. 13 to a plot of $\log\langle r^2\rangle$ versus log t, and $D_{FPR}(w)$ is obtained from fitting Eqs. 5 and 6 to the recovery curve. The corresponding diffusion coefficients for normal diffusion are D_{RSQ}(norm) and D_{FPR}(norm). We use $D_{RSQ}(w)$ as the reference standard because it accounts for anomalous subdiffusion and uses all the data in the simulation. In contrast, FPR simulation is an utterly inefficient way to find a diffusion coefficient. One calculates random walks for a large number of tracers, and then throws away all the information except whether each tracer was in the bleach spot at a given time.

We find that $D_{FPR}(w)$ is a reasonable, though not perfect, approximation to $D_{RSQ}(w)$, but fitting anomalous subdiffusion with the equations for normal diffusion gives erroneous results. As shown in Fig. 6, the normal recovery equation gives a systematically bad fit to an anomalous recovery curve, so the resulting value of D_{FPR}(norm) is incorrect unless α is near 1. Similarly, if diffusion is anomalous at all times, a plot of $\langle r^2\rangle$ versus t is nonlinear, so fitting it with a straight line gives a slope that depends on the measurement time, and D_{RSQ}(norm) is time-dependent.

Histograms of $D_{FPR}(w)$ for the different anomalous subdiffusion models are shown in Fig. 9. The results for obstructed diffusion are shown as linear and logarithmic histograms, but for the fBm model, only log $D_{FPR}(w)$ is shown so that the entire family of curves can be shown on one plot. In all models the distribution of Γ is much broader than the distribution of $D_{FPR}(w)$, and is asymmetric.

For obstructed diffusion far from the percolation threshold, $D_{FPR}(w)$ reduces to D_{FPR}(norm), and even at the threshold the distributions are similar. Both of these distributions are much broader than the distribution of the reference $D_{RSQ}(w)$ because fewer data points are used. As $C \rightarrow C_P$, the distribution of D narrows in the linear plot (Fig. 9 *a*) and D crowds around zero, but the distributions of log $D_{FPR}(w)$ widen (Fig. 9 *b*). The logarithmic distributions are more relevant to experiment; if experimental diffusion coefficients covered such a wide range, one would change the

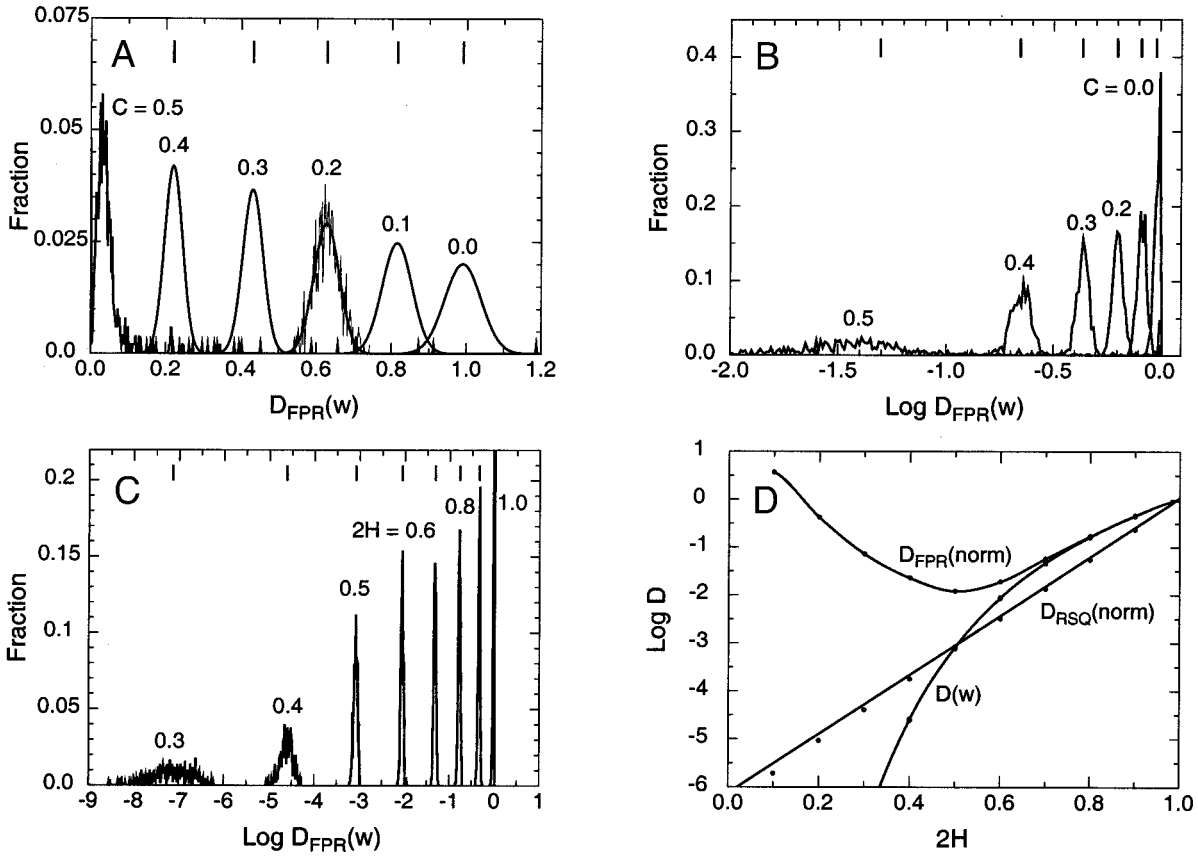

FIGURE 9 Diffusion coefficients $D_{FPR}(w)$ for simulated recovery curves fit by Eqs. 5 and 6. The short vertical lines in (*a–c*) are mean values. (*a*) Distributions of the diffusion coefficient $D_{FPR}(w)$ for obstructed diffusion with $C = 0.0$, 0.1, 0.2, 0.3, 0.4, and $C = C_P = 0.5$. The curves are Gaussians fit to the observed histograms; for two distributions, the actual histogram is shown as a fine line. Note the extreme tail for $C = 0.5$, extending beyond 1.2. (*b*) Distributions of log $D_{FPR}(w)$ for obstructed diffusion for the same values of C. (*c*) Distributions of log $D_{FPR}(w)$ for fBm with $2H = 0.3$, 0.4, 0.5, 0.6, 0.7, 0.8, 0.9, and 1.0. (*d*) Mean values of the various fBm diffusion coefficients as a function of $2H$. On the scale of this figure, $D_{RSQ}(w)$ and $D_{FPR}(w)$ are indistinguishable and are simply labeled $D(w)$. For D_{RSQ}(norm) a straight line fit at $2H = 0.9$ and 1.0 is shown; for the other diffusion coefficients, Catmull-Rom splines are used.

beam radius or the recording time to measure diffusion accurately. Anomalous behavior becomes important only for $C \geq 0.425$, as indicated by an increase in χ^2 for normal fits. At the percolation threshold, D_{FPR}(norm) and $D_{FPR}(w)$ occasionally show extremely high values. These are a result of eliminating the lakes, leaving just a few ocean sites at the edges of the bleach beam. Occasionally there are no ocean sites in the bleach beam.

For fBm, the distributions of $D_{FPR}(w)$ broaden considerably as $2H$ decreases, as shown in Fig. 9 *c*. Mean values of the various fBm diffusion coefficients are shown in Fig. 9 *d*. The values of $D_{RSQ}(w)$ and $D_{FPR}(w)$ are indistinguishable on the scale of the figure and are simply labeled $D(w)$. $D_{FPR}(w)$ is systematically higher by 3.5 to 7% for $2H \geq 0.4$. For moderately anomalous subdiffusion, $2H \geq 0.7$, D_{FPR}(norm) agrees well with $D(w)$, but at smaller $2H$ it systematically deviates, increasing sharply and spuriously when $2H$ decreases below 0.5. The value D_{RSQ}(norm) from the slope of $\langle r^2 \rangle$ versus t is in error except at $2H = 1$.

For the CTRW, the distributions of $D_{FPR}(w)$ decrease and broaden considerably as diffusion becomes more anomalous, just as shown for fBm. The mean values of the different diffusion coefficients are qualitatively similar to that shown in Fig. 9 *d*, except that the values of $D_{FPR}(w)$ are a factor of 0.4 to 0.8 smaller than values of $D_{RSQ}(w)$. Presumably this error in $D_{FPR}(w)$ results from the misfit shown in Fig. 6, *e* and *f*.

Fitting an anomalous recovery curve with the standard equation

Suppose that one fits an anomalous recovery curve using the standard form of the recovery curve for normal diffusion. The best example to use is fBm, where α can be varied over a wide range and the recovery curve is well-fit using Eqs. 5 and 6. The quality of fit is measured by χ^2 per time point. As shown in Fig. 10, as diffusion becomes more anomalous,

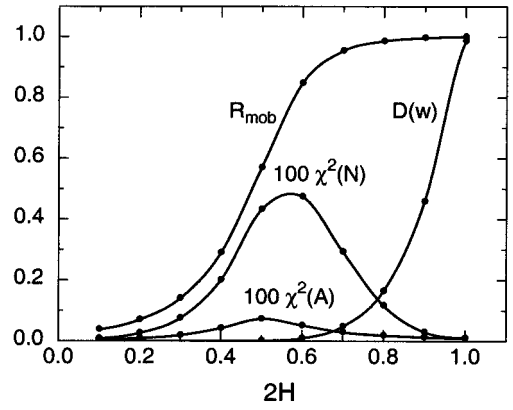

FIGURE 10 Results of fitting anomalous recovery curves for fBm with the normal recovery equation. Here R_{mob} is the apparent mobile fraction; $\chi^2(N)$ and $\chi^2(A)$ are the values of the mean-square error per point for fits to the normal and anomalous curves. For reference, the diffusion coefficient $D_{FPR}(w)$ is also given. Results are shown as points fit by Catmull-Rom splines.

the apparent mobile fraction R_{mob} from a fit to the standard curve decreases, and the quality of the fit by the standard curve becomes considerably worse. (The decrease in χ^2 for the standard fit for $2H \leq 0.5$ is misleading; if one examined the standard and anomalous fits one would immediately reject the standard fit.) The corresponding results for the CTRW for $\beta = 0.3$ to 0.9 are qualitatively similar. The anomalous curve fits better, as shown by values of χ^2 a factor of 25 lower than those for the normal recovery curve. The corresponding results for obstructed diffusion show that anomalous behavior becomes important only for $C \geq 0.425$, indicated by an increase in χ^2 for the normal fit.

If an anomalous recovery curve is fit using the standard equation, the results depend strongly on the number of time points included, as shown by Nagle (1992), but if the curve is fit using the anomalous equation, accurate values of α and reasonable values of $D(w)$ are obtained. For fBm with $2H = 0.5$, seven runs were made with the number of time points from 32K to 128M increasing by factors of 4. (For runs with 2M time points or fewer, there was no breakpoint and the recovery curve was entirely in the initial region described by Eq. 8.) As the run lengths increased, the diffusion coefficients based on normal diffusion, D_{RSQ}(norm) and D_{FPR}(norm), were strongly dependent on the run time, and decreased by factors of 58 and 220, respectively. In contrast, fits assuming anomalous subdiffusion gave good values of α for all run lengths, 0.501 from $\langle r^2(t)\rangle$ and 0.504 from the recovery curves, with standard deviations below 0.001. Values of $D_{RSQ}(w)$ and $D_{FPR}(w)$ agreed well, with $D_{FPR}(w)$ ~6% higher, and the standard deviations for the seven runs were 18% of the mean for both of these diffusion coefficients. The errors χ^2 per point were much larger for the normal fit than for the anomalous fit (by a factor of 2.6 to 22) and the bad fits were evident in a log-log plot of the recovery curve. Just as in the one-dimensional model of Nagle (1992), the standard equation yielded a mobile fraction strongly dependent on the number of time points in the recovery curve, here increasing from 25% to 90% mobile as the run time increased. The anomalous recovery curve can extrapolate the recovery curve reasonably well; a run with 512K points had a value of only 0.45 at the final time point, but a fit to a three-parameter anomalous recovery curve (α, Γ, and R_{mob}) gave a mobile fraction of 0.96 $\pm$ 0.12.

DISCUSSION

The main result is that according to the simulations, the effect of anomalous subdiffusion on FPR can usually be taken into account by the simple approximation of Eq. 5. To test for anomalous subdiffusion, one ought to fit the recovery curves by normal and anomalous equations and look for systematic deviations, both in linear plots to see the fit at large times and log-log plots to see the fit at short times. The improvement in fit to an anomalous recovery curve on fitting with the anomalous function is clear in the values of χ^2, but looking at the plots is far more informative, especially in view of the differences in shape of the recovery curves among different models of anomalous subdiffusion. Note that experimental limitations may affect observed recovery curves at short and long times. At short times the curve may be distorted by diffusion during the bleach pulse, imperfections in the beam profile, and limits in the rate of data collection; and at long times by motion of the membrane and photobleaching by the probe beam. As shown by Wolf (1989) and Gordon et al. (1995), among others, in fitting the recovery curves one ought to use a nonlinear least-squares fit to the full recovery curve, not a linearized approximation.

In anomalous subdiffusion, the diffusion coefficient is distance-dependent, but it is useful to have a single number with the dimensions of a diffusion coefficient to characterize diffusion, so we have defined $D_{FPR}(w)$ self-consistently in Eq. 15 to describe diffusion over distances of the order of the measurement distance w.

The simulation is sensitive to the choice of anomalous subdiffusion model. Requiring anomalous subdiffusion merely specifies the asymptotic value of one moment: $\langle r^2\rangle \sim t^\alpha$. The percolation, fBm, and CTRW models differ appreciably in their approach to the asymptotic value (Fig. 7) and in their noise levels (Figs. 4 and 5). Which model is appropriate depends on the mechanisms responsible for anomalous subdiffusion in the membrane. Despite the oscillations that are evident in linear plots of $\langle r^2(t)\rangle$ and obvious in log-log plots, fractional Brownian motion is the purest of the anomalous subdiffusion models used here and the fBm recovery curves are fit very well using Eqs. 5 and 6. For obstructed diffusion, the anomalous subdiffusion exponent α varies from 1 in the unobstructed system to 0.697 at the percolation threshold. The CTRW and fBm

models, like some of the binding models (Saxton, 1996) not discussed here, allow diffusion to be much more anomalous than pure obstruction does. Obstruction alone cannot account for the highly anomalous diffusion cited in the Introduction.

There is good reason to use the approximation of Feder et al. (1996). It is an asymptotic approximation that describes a major part of the behavior of anomalous subdiffusion, though not all. Fig. 7 shows the nature of the approximation; the families of curves in Fig. 2 and the fits in Figs. 6 show that this approximation describes anomalous recovery curves better because the initial time dependence is $F(t) \propto t^{\alpha/2}$. Anomalous subdiffusion explains the linear ramp that Vaz et al. (1989) included on physical grounds, and predicts that in obstructed systems it is important only near the percolation threshold. The threshold is observable in FPR not only as a transition in the mobile fraction, but also as an increase in noise in the shape of the recovery curve (Fig. 5) and a broadening in the distributions of α and $\log D$ (Figs. 8 and 9). Scatter in FPR and SPT (Saxton, 1997) should be viewed as both signal and noise; here the noise is a signature of the percolation threshold. It is therefore useful for experimentalists to publish histograms of diffusion coefficients, not just mean values with an often disturbingly large standard deviation.

In the simulations we have excluded diffusion in lakes. Lakes can be eliminated experimentally by a prebleach (Schwille et al., 1999a). If lakes are included, it is necessary to include the mobile fraction as a third parameter in the anomalous fits. Without this the fits are clearly erroneous because the anomalous function goes to one at large times and the actual recovery curve does not. In experiments on lipid mixtures it is necessary to include the mobile fraction if the lakes are stable on the time scale of the measurement. The stability of the obstacles is demonstrated by the observation that in a mixture of dimyristoylphosphatidylcholine and distearoylphosphatidylcholine, 20% gel phase by mass disconnects 80% fluid phase (Vaz et al., 1989). In experiments on cells, Feder et al. (1996) found that a three-parameter fit including an immobile fraction worked better than a fit with just Γ and α.

Vaz, Thompson, Almeida, and collaborators (for reviews see Vaz, 1992; Almeida and Vaz, 1995) interpreted their FPR measurements in two-phase and three-phase lipid mixtures in terms of percolation of the fluid phase. The modeling of FPR presented here is consistent with their analysis.

The obstruction model may appear to be of limited biological use, restricted to artificial bilayers with a lateral phase separation between gel and fluid phases. As Almeida et al. (1992a) pointed out, obstruction and percolation are also applicable to liquid-liquid lateral phase separation, as in the liquid-ordered and liquid-disordered phases. There has been much interest lately in lipid rafts, considered to be domains of liquid-ordered phase, and their role in signal transduction (Brown and London, 2000; London and Brown, 2000; Simons and Ikonen, 2000; Simons and Toomre, 2000). Rietveld and Simons (1998) suggested that in most membranes the liquid-disordered phase percolates, but that in the apical membrane of polarized epithelial cells the liquid-ordered phase percolates. If a mobile species has a very strong preference for one of the phases, percolation could have a major effect on its motion, so it would be of considerable interest to measure the partition coefficients for proteins involved in signaling reactions.

APPENDIX

Equations for the recovery curves

Axelrod et al. (1976) give the recovery curve for a uniform circular bleach spot as

$$F_A(z) = F_A^0(z) - S(z), \tag{A1}$$

where

$$F_A^0(z) = 1 - \frac{z}{2} e^{-z}[I_0(z) + I_2(z)] \tag{A2}$$

and

$$S(z) = 2\sum_{k=0}^{\infty} \frac{(2k+2)!(k+1)!}{(k!)^2[(k+2)!]^2} \left(-\frac{z}{2}\right)^k. \tag{A3}$$

Here $z = 2\tau_D/t$, $\tau_D = w^2/4D$ is the recovery time, w is the beam radius, D is the diffusion coefficient, and $I_\nu(z)$ is a modified Bessel function. The sign of the series has been corrected according to Lopez et al. (1988). Soumpasis (1983) gives the form

$$F_S(z) = e^{-z}[I_0(z) + I_1(z)]. \tag{A4}$$

It would be reassuring to know that these are the same. As a preliminary test, F_A and F_S were expanded as a 10-term power series in z using Mathematica (Wolfram, 1999) and were found to agree. We outline the proof that the series are equal. Clearly, it will be useful to have a power series expansion of $e^{-z}I_\nu(z)$. We use Eq. 13.6.3 of Abramowitz and Stegun (1972) to write this as a Kummer function

$$M(\nu + 1/2, 2\nu + 1, 2z) = \Gamma(\nu + 1)(2/z)^\nu e^z I_\nu(z), \tag{A5}$$

where $\Gamma(\nu)$ is the gamma function. We then replace z with $-z$ and use the fact that $I_\nu(-z) = (-1)^\nu I_\nu(z)$ (Abramowitz and Stegun, 1972, Eq. 9.6.30) to obtain

$$e^{-z}I_\nu(z) = \frac{1}{\Gamma(\nu+1)} \left(\frac{z}{2}\right)^\nu M(\nu + 1/2, 2\nu + 1, 2z). \tag{A6}$$

The series expansion of the Kummer function is given by Eqs. 13.1.2 and 6.1.22 of Abramowitz and Stegun (1972), and we obtain

$$e^{-z}I_\nu(z) = \frac{\Gamma(2\nu+1)}{\Gamma(\nu+1)\Gamma(\nu+1/2)} \left(\frac{z}{2}\right)^\nu \cdot \sum_{n=0}^{\infty} \frac{(-2z)^n}{n!} \frac{\Gamma(n+\nu+1/2)}{\Gamma(n+2\nu+1)}. \tag{A7}$$

We then substitute Eq. A7 into Eqs. A1, A2, and A4, and use standard identities for gamma functions and factorials (Abramowitz and Stegun, 1972, Chapter 6) to show that $F_A(z) = F_S(z)$. It is convenient to do this by finding the general term of the power series for $F_A^0 - F_S$, reducing it to its simplest form, and then showing it is equal to the simplest form of the general term in Eq. A3.

I thank Paulo Almeida and Watt Webb for helpful discussions, and the reviewers for useful suggestions.

This work was supported by National Institutes of Health Grant GM38133.

REFERENCES

Abramowitz, M., and I. A. Stegun. 1972. Handbook of Mathematical Functions. U.S. Government Printing Office, Washington, D.C.

Almeida, P. F. F., and W. L. C. Vaz. 1995. Lateral diffusion in membranes. *In* Structure and Dynamics of Membranes. R. Lipowsky and E. Sackmann, editors. Vol. 1. Elsevier Science, Amsterdam. 305–357.

Almeida, P. F. F., W. L. C. Vaz, and T. E. Thompson. 1992a. Lateral diffusion in the liquid phases of dimyristoylphosphatidylcholine/cholesterol lipid bilayers: a free volume analysis. *Biochemistry.* 31: 6739–6747.

Almeida, P. F. F., W. L. C. Vaz, and T. E. Thompson. 1992b. Lateral diffusion and percolation in two-phase, two-component lipid bilayers: topology of the solid-phase domains in-plane and across the lipid bilayer. *Biochemistry.* 31:7198–7210.

Almeida, P. F. F., W. L. C. Vaz, and T. E. Thompson. 1993. Percolation and diffusion in three-component lipid bilayers: effect of cholesterol on an equimolar mixture of two phosphatidylcholines. *Biophys. J.* 64: 399–412.

Axelrod, D., D. E. Koppel, J. Schlessinger, E. Elson, and W. W. Webb. 1976. Mobility measurement by analysis of fluorescence photobleaching recovery kinetics. *Biophys. J.* 16:1055–1069.

Berry, M. V., and Z. V. Lewis. 1980. On the Weierstrass-Mandelbrot fractal function. *Proc. R. Soc. (Lond.) A.* 370:459–484.

Blumen, A., J. Klafter, B. S. White, and G. Zumofen. 1984. Continuous-time random walks on fractals. *Phys. Rev. Lett.* 53:1301–1304.

Bouchaud, J.-P., and A. Georges. 1988. The physical mechanisms of anomalous diffusion. *In* Disorder and Mixing. E. Guyon, J.-P. Nadal, and Y. Pomeau, editors. Kluwer Academic Publishers, Dordrecht, The Netherlands. 19–29.

Bouchaud, J.-P., and A. Georges. 1990. Anomalous diffusion in disordered media: statistical mechanisms, models and physical applications. *Phys. Reports.* 195:127–293.

Brown, D. A., and E. London. 2000. Structure and function of sphingolipid- and cholesterol-rich membrane rafts. *J. Biol. Chem.* 275: 17221–17724.

Bunde, A., and S. Havlin. 1991. Percolation I. *In* Fractals and Disordered Systems. A. Bunde and S. Havlin, editors. Springer-Verlag, Berlin. 50–95.

Caccia, D. C., D. Percival, M. J. Cannon, G. Raymond, and J. B. Bassingthwaighte. 1997. Analyzing exact fractal time series: evaluating dispersional analysis and rescaled range methods. *Physica A.* 246:609–632.

Cherry, R. J., P. R. Smith, I. E. G. Morrison, and N. Fernandez. 1998. Mobility of cell surface receptors: a re-evaluation. *FEBS Lett.* 430: 88–91.

Coelho, F. P., W. L. C. Vaz, and E. Melo. 1997. Phase topology and percolation in two-component lipid bilayers: a Monte Carlo approach. *Biophys. J.* 72:1501–1511.

Donaldson, P. J. 1989. Modulation of lateral diffusion on lipid bilayer membranes. Ph.D. thesis, Cornell University, Ithaca, NY.

Edidin, M. 1996. Getting there is only half the fun. *Curr. Topics Membr.* 43:1–13.

Edidin, M. 1997. Lipid microdomains in cell surface membranes. *Curr. Opin. Struct. Biol.* 7:528–532.

Falconer, K. J., and J. L. Véhel. 2000. Horizons of fractional Brownian surfaces. *Proc. R. Soc. (Lond.) A.* 456:2153–2178.

Feder, J. 1988. Fractals. Plenum Press, New York. 170–178.

Feder, T. J., I. Brust-Mascher, J. P. Slattery, B. Baird, and W. W. Webb. 1996. Constrained diffusion or immobile fraction on cell surfaces: a new interpretation. *Biophys. J.* 70:2767–2773.

Foley, J. D., A. van Dam, S. K. Feiner, and J. F. Hughes. 1990. Computer Graphics: Principles and Practice. 2nd Ed. Addison-Wesley, Reading, MA. 504–507.

Ghosh, R. N. 1991. Mobility and clustering of individual low density lipoprotein receptor molecules on the surface of human skin fibroblasts. Ph.D. thesis, Cornell University, Ithaca, NY.

Ghosh, R. N., and W. W. Webb. 1994. Automated detection and tracking of individual and clustered cell surface low density lipoprotein receptor molecules. *Biophys. J.* 66:1301–1318.

Gordon, G. W., B. Chazotte, X. F. Wang, and B. Herman. 1995. Analysis of simulated and experimental fluorescence recovery after photobleaching: data for two diffusing components. *Biophys. J.* 68: 766–778.

Haus, J. W., and K. W. Kehr. 1987. Diffusion in regular and disordered lattices. *Phys. Rep.* 150:263–406.

Havlin, S., and D. Ben-Avraham. 1987. Diffusion in disordered media. *Adv. Phys.* 36:695–798.

Havlin, S., and A. Bunde. 1991. Percolation II. *In* Fractals and Disordered Systems. A. Bunde and S. Havlin, editors. Springer-Verlag, Berlin. 96–149.

Hoshen, J., and R. Kopelman. 1976. Percolation and cluster distribution. I. Cluster multiple labelling technique and critical concentration algorithm. *Phys. Rev. B.* 14:3438–3445.

Jacobson, K., and C. Dietrich. 1999. Looking at lipid rafts? *Trends Cell Biol.* 9:87–91.

Jaggard, D. L. 1990. On fractal electrodynamics. *In* Recent Advances in Electromagnetic Theory. H. N. Kritikos and D. L. Jaggard, editors. Springer-Verlag, New York. 183–225.

Jennane, R., R. Harba, and G. Jacquet. 1996. Quality of synthesis and analysis methods for fractional Brownian motion. *In* 1996 IEEE Digital Signal Processing Workshop Proceedings. J. M. Lervik and P. Waldemar, editors. IEEE, New York. 307–310.

Kirkpatrick, S., and E. P. Stoll. 1981. A very fast shift-register sequence random number generator. *J. Comput. Phys.* 40:517–526.

Kusumi, A., and Y. Sako. 1996. Cell surface organization by the membrane skeleton. *Curr. Opin. Cell Biol.* 8:566–574.

London, E., and D. A. Brown. 2000. Insolubility of lipids in Triton X-100: physical origin and relationship to sphingolipid/cholesterol membrane domains (rafts). *Biochim. Biophys. Acta.* 1508:182–195.

Lopez, A., L. Dupou, A. Altibelli, J. Trotard, and J.-F. Tocanne. 1988. Fluorescence recovery after photobleaching (FRAP) experiments under conditions of uniform disk illumination: critical comparison of analytical solutions, and a new mathematical method for calculation of diffusion coefficient D. *Biophys. J.* 53:963–970.

Lundahl, T., W. J. Ohley, S. M. Kay, and R. Siffert. 1986. Fractional Brownian motion: a maximum likelihood estimator and its application to image texture. *IEEE Trans. Medical Imaging.* MI-5:152–161.

Molz, F. J., and G. K. Boman. 1995. Further evidence of fractal structure in hydraulic conductivity distributions. *Geophys. Res. Lett.* 22: 2545–2548.

Molz, F. J., H. H. Liu, and J. Szulga. 1997. Fractional Brownian motion and fractional Gaussian noise in subsurface hydrology: a review, presentation of fundamental properties, and extensions. *Water Resources Research.* 33:2273–2286.

Munnelly, H. M., D. A. Roess, W. F. Wade, and B. G. Barisas. 1998. Interferometric fringe fluorescence photobleaching recovery interrogates entire cell surfaces. *Biophys. J.* 75:1131–1138.

Nagle, J. F. 1992. Long tail kinetics in biophysics? *Biophys. J.* 63: 366–370.

Petersen, N. O., S. Felder, and E. L. Elson. 1986. Measurement of lateral diffusion by fluorescence photobleaching recovery. *In* Handbook of

Experimental Immunology, Vol. 1, Immunochemistry, 4th Ed. D. M. Weir, editor. Blackwell Scientific Publications, Oxford. 24.1–24.23.

Press, W. H., S. A. Teukolsky, W. T. Vetterling, and B. P. Flannery. 1992. Numerical Recipes in Fortran: The Art of Scientific Computing, 2nd Ed. Cambridge University Press, Cambridge.

Rietveld, A., and K. Simons. 1998. The differential miscibility of lipids as the basis for the formation of functional membrane rafts. *Biochim. Biophys. Acta.* 1376:467–479.

Saxton, M. J. 1994. Anomalous diffusion due to obstacles: a Monte Carlo study. *Biophys. J.* 66:394–401.

Saxton, M. J. 1996. Anomalous diffusion due to binding: a Monte Carlo study. *Biophys. J.* 70:1250–1262.

Saxton, M. J. 1997. Single-particle tracking: the distribution of diffusion coefficients. *Biophys. J.* 72:1744–1753.

Saxton, M. J. 1999. Lateral diffusion of lipids and proteins. *Curr. Topics Membr.* 48:229–282.

Saxton, M. J., and K. Jacobson. 1997. Single-particle tracking: applications to membrane dynamics. *Annu. Rev. Biophys. Biomol. Struct.* 26: 373–399.

Scalettar, B. A., and J. R. Abney. 1991. Molecular crowding and protein diffusion in biological membranes. *Comments Mol. Cell. Biophys.* 7:79–107.

Scher, H., M. F. Shlesinger, and J. T. Bendler. 1991. Time-scale invariance in transport and relaxation. *Phys. Today.* 44(1):26–34.

Schram, V., H.-N. Lin, and T. E. Thompson. 1996. Topology of gel-phase domains and lipid mixing properties in phase-separated two-component phosphatidylcholine bilayers. *Biophys. J.* 71:1811–1822.

Schram, V., J.-F. Tocanne, and A. Lopez. 1994. Influence of obstacles on lipid lateral diffusion: computer simulation of FRAP experiments and application to proteoliposomes and biomembranes. *Eur. Biophys. J.* 23:337–348.

Schwille, P., U. Haupts, S. Maiti, and W. W. Webb. 1999a. Molecular dynamics in living cells observed by fluorescence correlation spectroscopy with one- and two-photon excitation. *Biophys. J.* 77:2251–2265.

Schwille, P., J. Korlach, and W. W. Webb. 1999b. Fluorescence correlation spectroscopy with single-molecule sensitivity on cell and model membranes. *Cytometry.* 36:176–182.

Sheets, E. D., G. M. Lee, R. Simson, and K. Jacobson. 1997. Transient confinement of a glycosylphosphatidylinositol-anchored protein in the plasma membrane. *Biochemistry.* 36:12449–12458.

Shlesinger, M. F. 1988. Fractal time in condensed matter. *Annu. Rev. Phys. Chem.* 39:269–290.

Simons, K., and E. Ikonen. 2000. How cells handle cholesterol. *Science.* 290:1721–1726.

Simons, K., and D. Toomre. 2000. Lipid rafts and signal transduction. *Nature Rev. Mol. Cell Biol.* 1:31–39; 2:216.

Simson, R., B. Yang, S. E. Moore, P. Doherty, F. S. Walsh, and K. A. Jacobson. 1998. Structural mosaicism on the submicron scale in the plasma membrane. *Biophys. J.* 74:297–308.

Slattery, J. P. 1995. Lateral mobility of $Fc_{\epsilon}RI$ on rat basophilic leukemia cells as measured by single particle tracking using a novel bright fluorescent probe. Ph.D. thesis, Cornell University, Ithaca, NY.

Smith, P. R., I. E. G. Morrison, K. M. Wilson, N. Fernández, and R. J. Cherry. 1999. Anomalous diffusion of major histocompatibility complex class I molecules on HeLa cells determined by single particle tracking. *Biophys. J.* 76:3331–3344.

Soumpasis, D. M. 1983. Theoretical analysis of fluorescence photobleaching recovery experiments. *Biophys. J.* 41:95–97.

Stauffer, D., and A. Aharony. 1992. Introduction to Percolation Theory, 2nd Ed. Taylor & Francis, London. 33; 49–50.

Thomas, J., and W. W. Webb. 1990. Fluorescence photobleaching recovery: a probe of membrane dynamics. *In* Noninvasive Techniques in Cell Biology. J. K. Foskett and S. Grinstein, editors. Wiley-Liss, New York. 129–152.

Vaz, W. L. C. 1992. Translational diffusion in phase-separated lipid bilayer membranes. *Comments Mol. Cell. Biophys.* 8:17–36.

Vaz, W. L. C., E. C. C. Melo, and T. E. Thompson. 1989. Translational diffusion and fluid domain connectivity in a two-component, two-phase phospholipid bilayer. *Biophys. J.* 56:869–876.

Voss, R. F. 1988. Fractals in nature: from characterization to simulation. *In* The Science of Fractal Images. H.-O. Peitgen and D. Saupe, editors. Springer-Verlag, New York. 21–70.

Wolf, D. E. 1989. Designing, building, and using a fluorescence recovery after photobleaching instrument. *Methods Cell Biol.* 30:271–306.

Wolfram, S. 1999. The Mathematica Book, 4th Ed. Wolfram Media/ Cambridge University Press, Cambridge.